

Reinforced Concrete Frame Element with Bond Interfaces. II: State Determinations and Numerical Validation

Suchart Limkatanyu¹ and Enrico Spacone²

Abstract: This is the second of two papers discussing the theories and applications of three reinforced concrete (RC) frame elements with bond slip between the reinforcing bars and the concrete. This paper presents the element state determinations for the displacement-based, the force-based, and the Hellinger–Reissner mixed formulations. The convergence, accuracy, and computational times of the three elements are compared through two numerical examples. The distinctive element characteristics in terms of force and deformation discontinuities between adjacent elements are discussed for the three proposed formulations. The ability of these formulations to detect the overall softening response of RC members due to the pullout failure of the rebars in the anchorage zone is also tested. The elements are all able to capture the drop in member stiffness due to the rebar slip and the failure due to bar pullout. The force-based and the mixed elements are, however, much more precise than the displacement-based element. The force-based element is slightly more precise, but the mixed element is numerically more stable.

DOI: 10.1061/(ASCE)0733-9445(2002)128:3(356)

CE Database keywords: Concrete; Reinforced; Frames; Bonding; Beams; Finite elements; Nonlinear analysis.

Introduction

In recent years, several researchers have investigated the use of assumed force fields for the development of nonlinear frame elements. This interest stems from two main observations: (1) in some simplified cases the internal force distributions in frame elements are known “exactly.” This is, for example, the case of the reinforced concrete (RC) beam element with perfect bond; (2) in general, the force fields along the beam are smoother than the deformation fields, which may show large jumps in the inelastic regions, particularly where plastic hinges tend to form (i.e., in column bases, girder ends, beam midspan, etc.). While the development of elements that use force shape functions is per se simple, the implementation of such elements in existing nonlinear structural analysis programs is the real challenge in the element formulation.

Mahasuverachai and Powell (1982) used the force-dependent shape functions to trace the inelastic response of pipes and tubular structures. Kaba and Mahin (1984) proposed the first fiber beam element, which uses force shape functions to compute the element flexibility and the displacement shape functions to compute the element resisting forces. The element yielded promising results but was hampered by convergence problems, especially for softening materials such as concrete. The element by Kaba and

Mahin (1984) was later improved by Zeris and Mahin (1988, 1991), but their procedure to compute the element stiffness matrix and the element-resisting forces was not entirely general and required an ad hoc approach to solve softening problems.

The main problem in implementing elements that exclusively use force shape functions (i.e., force-based elements) or that mix displacement and force shape functions (i.e., mixed elements) derives from the displacement-based nature of the nonlinear solution schemes used in structural analysis. The assumption of force shape functions naturally leads to the element flexibility and to the element displacements that are compatible with the internal deformation distributions (in beams, these are primarily the axial strain and the curvature). However, the nonlinear structural solution schemes typically necessitate the element stiffness and the element forces corresponding to the current nodal displacements.

Ciampi and Carlesimo (1986) were the first to propose the consistent formulation of force-based elements. Their procedure was refined by Spacone et al. (1996) to develop a force-based fiber frame element for the nonlinear analysis of RC structures. The element by Spacone et al. (1996) assumes a perfect bond between the concrete and the rebars, hence leading to an internally statically determinate element. The force shape functions are easily derived from equilibrium and are “exact” within the Euler–Bernoulli beam theory.

For members that are internally statically indeterminate (such as steel–concrete composite elements with deformable shear studs and RC frame elements with bond slip), the derivation of the equilibrated force shape functions is not trivial. Salari et al. (1998) proposed a procedure to derive the equilibrated force shape functions for the steel–concrete composite element with deformable shear studs. The refined version of the element state determination by Salari et al. (1998) is used for the forced-based RC frame element proposed in this study. Ayoub and Filippou (2000) used both force and displacement shape functions to develop a mixed composite frame element with deformable shear studs.

¹Lecturer, Dept. of Civil Engineering, Prince of Songkla Univ., Hadyai 90110, Thailand.

²Associate Professor, Dept. of Civil, Environmental and Architectural Engineering, Univ. of Colorado, Boulder, CO 80309-0428. E-mail: spacone@colorado

Note. Associate Editor: Marc I. Hoit. Discussion open until August 1, 2002. Separate discussions must be submitted for individual papers. To extend the closing date by one month, a written request must be filed with the ASCE Managing Editor. The manuscript for this paper was submitted for review and possible publication on February 21, 2001; approved on August 17, 2001. This paper is part of the *Journal of Structural Engineering*, Vol. 128, No. 3, March 1, 2002. ©ASCE, ISSN 0733-9445/2002/3-356–364/\$8.00+\$5.50 per page.

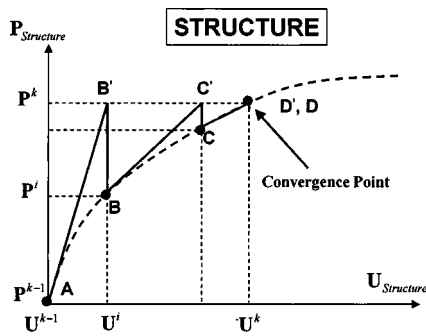


Fig. 1. Nodal Newton–Raphson solution scheme for load step

The element state determinations for the displacement-based, force-based, and Hellinger–Reissner (H–R) mixed RC frame elements with bond slip presented in the companion paper by Limkatanyu and Spacone (2002) are the first items discussed in this paper. Next, the convergence, accuracy, computational time, and distinctive characteristics of the three types of elements are discussed through two numerical examples. Finally, the ability of the proposed elements to represent the overall softening response of RC members with insufficient anchorage lengths is studied.

Element State Determinations

The elements proposed in this work are implemented in the general-purpose finite element code FEAP (Taylor 2000). A typical Newton–Raphson scheme for each of the three element state determinations is described herein. It should be noted that any other nonlinear global solution scheme can be followed. The nonlinear program solver compares applied and resisting forces and detects whether equilibrium has been reached, or whether further steps are needed. One load step, labeled k , is schematically shown in Fig. 1. Superscript i indicates the Newton–Raphson step. Based on the applied load vector \mathbf{P}^k and the current tangent stiffness matrix, B' , C' , and D' represent the predictor points. B , C , and D are the corrector points, and represent the nodal forces in equilibrium with the element resisting forces that correspond to the current nodal displacements. The final converged displacement vector is labeled \mathbf{U}^k .

In a nonlinear structural analysis program, the element routines are responsible for computing the element forces and the element stiffness corresponding to the current nodal displacements. This procedure is sometimes called element state determination. The step-by-step element state determinations of the three frame element formulations presented in Limkatanyu and Spacone (2002) are discussed hereafter. The steps involved in the three state determinations are summarized in Table 1.

Displacement-Based Element

The state determination for the displacement-based element is by far the simplest, because the element formulation and the nonlinear solution algorithms of the finite element code at the structural degrees of freedom are both displacement based.

The first column in Table 1 summarizes the steps followed in the implementation of the proposed displacement-based RC frame element with bond slip. The procedure is also shown in Fig. 2, which schematically represents the element, beam section, and bond state determinations. The current section deformations \mathbf{d}_B

and the current bond deformations \mathbf{d}_b are computed from the current element nodal displacements \mathbf{U} via the derivatives of the displacement shape functions (step c in Table 1, column 1). Based on the current section and bond deformations, the section and bond state determinations are performed to compute the current section stiffness \mathbf{k}_B and bond stiffness \mathbf{k}_b , as well as the section forces \mathbf{D}_{BR} and the bond forces \mathbf{D}_{bR} (step d). Next, the current element stiffness matrix \mathbf{K} is calculated from the current section stiffness and bond stiffness matrices (step f). Finally, based on the current section and bond resisting forces, the current element resisting forces \mathbf{Q} are computed (step h).

In the displacement-based state determination, element compatibility is satisfied pointwise along the element, for both the beam and the bond, because the section and bond deformations are found from the displacement shape functions. On the other hand, element equilibrium is only satisfied in an integral sense, because the element forces are found as integrals of the section and bond forces.

Force-Based (Force-Hybrid) Element

This is the most challenging element to implement, because the element resisting forces cannot be directly computed from the section resisting forces. This is a well-known issue in force-based elements. Their implementation in a displacement-based finite element program requires a hybrid approach where the element forces are computed from the element displacements and deformations. Over the years, the element state determination for force-based elements has evolved to include nonlinear strain-hardening as well as nonlinear strain softening material behavior. The present work uses the approach initially proposed by Spacone et al. (1996) for elements with perfect bond and later extended by Salari et al. (1998) to steel–concrete composite elements with deformable shear studs. The original approach by Spacone et al. (1996) involves a Newton–Raphson iterative scheme at the element level that is based on the nodal residual deformations. The compatible configuration is reached when the integral of the section deformations equals (within a prescribed tolerance) the current nodal displacements computed by the finite element solver. Neuenhofer and Filippou (1997) proposed a simplified procedure where the iterations are truncated after a first approximation of the element forces is found, thus relying on the iterations at the structural degrees of freedom to find nodal equilibrium and element compatibility. The two approaches are very similar. The first one is more precise, but computationally more demanding.

The second column in Table 1 shows the steps followed in the implementation of the proposed force-based RC frame element with bond slip. The element forces and deformations are all computed without rigid body modes, and the notation used in the companion paper (Limkatanyu and Spacone 2002) should be followed. The element arrays should be written $\bar{\mathbf{Q}}$, $\bar{\mathbf{F}}$, $\bar{\mathbf{K}}$, $\bar{\mathbf{U}}$, $\bar{\mathbf{r}}$, but for the sake of brevity the bar is omitted. The hybrid state determination is also shown in Fig. 3, which schematically represent the element, section, and bond state determinations.

The first step is to compute the element force increments $\Delta\mathbf{Q}$ and the reference bond force increments $\Delta\mathbf{Q}_b$ by linearizing the element force–deformation relation about the initial point 0 (step a in Table 1, column 2). The current section forces \mathbf{D}_B and bond forces \mathbf{D}_b are found using the force shape functions (step b). The section and bond deformations \mathbf{d}_B and \mathbf{d}_b are found by consistent linearization of the force–deformation relation about the initial point (step c). Based on \mathbf{d}_B and \mathbf{d}_b , the section and bond state determinations are performed to compute the current section stiff-

Table 1. Steps in element state determinations ($\mathbf{A}_b = -\mathbf{F}_{bb}^{-1}\mathbf{F}_{bB}$, $\mathbf{N}_{Br}^{FB} = \mathbf{N}_{BB}^{FB} + \mathbf{N}_{Bb}^{FB}\mathbf{A}_b$, $\mathbf{N}_{br}^{FB} = \mathbf{N}_{BB}^{FB} + \mathbf{N}_{bb}^{FB}\mathbf{A}_b$)

Step	Displacement-based algorithm	Force-based algorithm	Mixed algorithm
(a) Element force increment		$\Delta \mathbf{Q} = \mathbf{K}^0 \Delta U$ $\Delta \mathbf{Q}_b = \mathbf{A}_b^0 \Delta \mathbf{Q} - (\mathbf{F}_{bb}^0)^{-1} \mathbf{r}_b^0$	$\Delta \mathbf{Q}_R = (\mathbf{F}_B^0)^{-1} \mathbf{T} \Delta U$
(b) Section and/or bond forces		$\Delta \mathbf{D}_B = \mathbf{N}_{BB}^{FB} \Delta \mathbf{Q} + \mathbf{N}_{Bb}^{FB} \Delta \mathbf{Q}_b$ $\Delta \mathbf{D}_b = \mathbf{N}_{bb}^{FB} \Delta \mathbf{Q} + \mathbf{N}_{Bb}^{FB} \Delta \mathbf{Q}_b$ $\mathbf{D}_B = \mathbf{D}_B^0 + \Delta \mathbf{D}_B$ $\mathbf{D}_b = \mathbf{D}_b^0 + \Delta \mathbf{D}_b$	$\Delta \mathbf{D}_B = \mathbf{N}_F^{H-R} \Delta \mathbf{Q}_R$ $\mathbf{D}_B = \mathbf{D}_B^0 + \Delta \mathbf{D}_B$
(c) Section and bond deformations	$\mathbf{d}_B = \mathbf{B}_B^{DB} \mathbf{U}$ $\mathbf{d}_b = \mathbf{B}_b^{DB} \mathbf{U}$	$\mathbf{d}_B = \mathbf{d}_B^0 + \mathbf{f}_B^0 \Delta \mathbf{D}_B$ $\mathbf{d}_b = \mathbf{d}_b^0 + \mathbf{f}_b^0 \Delta \mathbf{D}_b$	$\mathbf{d}_B = \mathbf{d}_B^0 + \mathbf{f}_B^0 \Delta \mathbf{D}_B$ $\mathbf{d}_b = \mathbf{B}_b^{H-R} \mathbf{U}$
(d) Section and bond state determination	$\mathbf{k}_B = \mathbf{k}_B(\mathbf{d}_B)$, $\mathbf{D}_{BR} = \mathbf{D}_{BR}(\mathbf{d}_B)$ $\mathbf{k}_b = \mathbf{k}_b(\mathbf{d}_b)$, $\mathbf{D}_{br} = \mathbf{D}_{br}(\mathbf{d}_b)$	$\mathbf{f}_B = \mathbf{k}_B^{-1}(\mathbf{d}_B)$, $\mathbf{D}_{BR} = \mathbf{D}_{BR}(\mathbf{d}_B)$ $\mathbf{f}_b = \mathbf{k}_b^{-1}(\mathbf{d}_b)$, $\mathbf{D}_{br} = \mathbf{D}_{br}(\mathbf{d}_b)$	$\mathbf{f}_B = \mathbf{k}_B^{-1}(\mathbf{d}_B)$, $\mathbf{D}_{BR} = \mathbf{D}_{BR}(\mathbf{d}_B)$ $\mathbf{k}_b = \mathbf{k}_b(\mathbf{d}_b)$, $\mathbf{D}_{br} = \mathbf{D}_{br}(\mathbf{d}_b)$
(e) Section and/or bond residual deformations		$\mathbf{d}_{Br} = \mathbf{f}_B(\mathbf{D}_B - \mathbf{D}_{BR})$ $\mathbf{d}_{br} = \mathbf{f}_b(\mathbf{D}_b - \mathbf{D}_{br})$	$\mathbf{d}_{Br} = \mathbf{f}_B(\mathbf{D}_B - \mathbf{D}_{BR})$
(f) Element stiffness	$\mathbf{K} = \int_L \mathbf{B}_B^{DBT} \mathbf{k}_B \mathbf{B}_B^{DB} dx + \int_L \mathbf{B}_b^{DBT} \mathbf{k}_b \mathbf{B}_b^{DB} dx$	$\mathbf{F}_{BB} = \int_L (\mathbf{N}_{BB}^{FBT} \mathbf{f}_B \mathbf{N}_{BB}^{FB} + \mathbf{N}_{Bb}^{FBT} \mathbf{f}_b \mathbf{N}_{Bb}^{FB}) dx$ $\mathbf{F}_{Bb} = \int_L (\mathbf{N}_{BB}^{FBT} \mathbf{f}_B \mathbf{N}_{Bb}^{FB} + \mathbf{N}_{Bb}^{FBT} \mathbf{f}_b \mathbf{N}_{Bb}^{FB}) dx$ $\mathbf{F}_{bb} = \int_L (\mathbf{N}_{Bb}^{FBT} \mathbf{f}_B \mathbf{N}_{Bb}^{FB} + \mathbf{N}_{bb}^{FBT} \mathbf{f}_b \mathbf{N}_{bb}^{FB}) dx$ $\mathbf{F} = \mathbf{F}_{BB} - \mathbf{F}_{Bb} \mathbf{F}_{bb}^{-1} \mathbf{F}_{Bb}^T$ $\mathbf{K} = (\mathbf{F})^{-1}$	$\mathbf{F}_B = \int_L \mathbf{N}_F^{H-RT} \mathbf{f}_B \mathbf{N}_F^{H-R} dx$ $\mathbf{K}_b = \int_L \mathbf{B}_b^{H-RT} \mathbf{k}_b \mathbf{B}_b^{H-R} dx$ $\mathbf{T} = \int_L \mathbf{N}_F^{H-RT} \mathbf{B}_B^{H-R} dx$ $\mathbf{K} = \mathbf{T}^T \mathbf{F}_B^{-1} \mathbf{T} + \mathbf{K}_b$
(g) Element residual deformations		$\mathbf{U}_r = \mathbf{U}_{Br} + \mathbf{U}_{br}$	$\mathbf{U}_{Rr} = \int_L \mathbf{N}_F^{H-RT} \mathbf{d}_B dx - \mathbf{TU}$
(h) Element forces	$\mathbf{Q} = \int_L \mathbf{B}_B^{DBT} \mathbf{D}_{BR} dx + \int_L \mathbf{B}_b^{DBT} \mathbf{D}_{br} dx$	$\mathbf{Q} = \mathbf{Q}^0 + \Delta \mathbf{Q} - \mathbf{K} \mathbf{U}_r$ $\mathbf{Q}_b = \mathbf{Q}_b^0 + \Delta \mathbf{Q}_b - \mathbf{A}_b \mathbf{K} \mathbf{U}_r$	$\mathbf{Q}_b = \int_L \mathbf{B}_b^{H-RT} \mathbf{D}_b dx$ $\mathbf{Q} = \mathbf{T}^T (\mathbf{Q}_R^0 + \Delta \mathbf{Q}_R) + \mathbf{Q}_b - \mathbf{T}^T (\mathbf{F}_B)^{-1} \mathbf{U}_{Rr}$
(i) Section and/or bond forces		$\mathbf{D}_B = \mathbf{D}_B - \mathbf{N}_{Br}^{FB} \mathbf{K} \mathbf{U}_r$ $\mathbf{D}_b = \mathbf{D}_b - \mathbf{N}_{br}^{FB} \mathbf{K} \mathbf{U}_r$	$\mathbf{D}_B = \mathbf{D}_B - \mathbf{N}_F^{H-R} \mathbf{F}_B^{-1} \mathbf{U}_{Rr}$
(j) Section and/or bond deformations		$\mathbf{d}_B = \mathbf{d}_B + \mathbf{d}_{Br} - \mathbf{f}_B \mathbf{N}_{Br}^{FB} \mathbf{K} \mathbf{U}_r$ $\mathbf{d}_b = \mathbf{d}_b + \mathbf{d}_{br} - \mathbf{f}_b \mathbf{N}_{br}^{FB} \mathbf{K} \mathbf{U}_r$	$\mathbf{d}_B = \mathbf{d}_B + \mathbf{d}_{Br} - \mathbf{f}_B \mathbf{N}_F^{H-R} \mathbf{F}_B^{-1} \mathbf{U}_{Rr}$

ness \mathbf{k}_B and bond stiffness \mathbf{k}_b , as well as the corresponding beam section \mathbf{D}_{BR} and bond \mathbf{D}_{br} resisting forces. The stiffness matrices are then inverted to compute the section flexibility \mathbf{f}_B and the bond flexibility \mathbf{f}_b (step d). The current section and bond residual deformations are found by transforming the corresponding force unbalances ($\mathbf{D}_B - \mathbf{D}_{BR}$ and $\mathbf{D}_b - \mathbf{D}_{br}$) into equivalent residual deformations \mathbf{d}_{Br} and \mathbf{d}_{br} (step e).

The current element flexibility matrix \mathbf{F} is computed from \mathbf{f}_B and \mathbf{f}_b , and is then inverted to get the current element stiffness matrix \mathbf{K} (step f). The current element residual deformations \mathbf{U}_r are the sum of the contributions of the current beam residuals \mathbf{U}_{Br} and of the current bond residual deformations \mathbf{U}_{br} (step g). The current forces \mathbf{Q} and \mathbf{Q}_b are then updated (step h). The current section and bond forces (\mathbf{D}_B and \mathbf{D}_b , respectively) are updated using the force shape functions (step i). Finally, the current sec-

tion deformations \mathbf{d}_B and bond slips \mathbf{d}_b are updated to reflect the changes in the corresponding forces (step j).

The element forces found with this procedure are not exact, but represent a first approximation. The “exact” forces are found when equilibrium at the nodal degrees of freedom is found. At this point, the vector of residual deformations \mathbf{U}_r approaches zero. This is the abbreviated procedure proposed by Neuenhofer and Filippou (1997). In the original hybrid procedure proposed by Spacone et al. (1996), the iterations continue by looping between steps *d* and *j* until the section residuals \mathbf{d}_{Br} and \mathbf{d}_{br} , and consequently the element residuals \mathbf{U}_{Br} and \mathbf{U}_{br} , approach zero. Finally, points *B**, *C**, and *D** in Fig. 3 are the predictor points of the procedure, while points *B*, *C*, and *D* are the final, corrector points of the solution step.

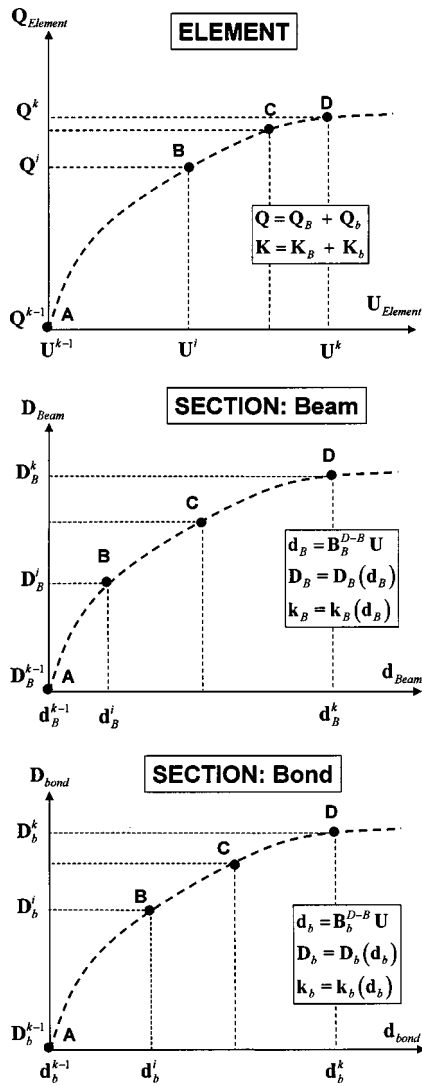


Fig. 2. Element state determination for displacement-based element

In the force-based state determination, force equilibrium is satisfied pointwise along the element because the element section forces are found from the equilibrated force shape functions, while compatibility of the element section deformations with the nodal displacements is only satisfied in an integral sense. This is the dual of the displacement-based state determination.

Hellinger–Reissner Mixed Element

The element state determination for the H–R mixed element is a hybrid between the displacement-based and the force-based state determinations. The bond state determination follows the displacement-based state determination, in that the bond slips are found from the nodal displacements via displacement shape functions. The beam state determination follows the force-based state determination, in that the section forces are computed from the nodal forces via force shape functions.

The last column of Table 1 shows the steps followed in the implementation of the proposed mixed RC frame element with bond slip. Similarly to the second column of Table 1 for the force-based element, for the sake of brevity the bar is omitted in the element arrays $\bar{\mathbf{F}}_B$ and $\bar{\mathbf{U}}_{Rr}$. The hybrid state determination is

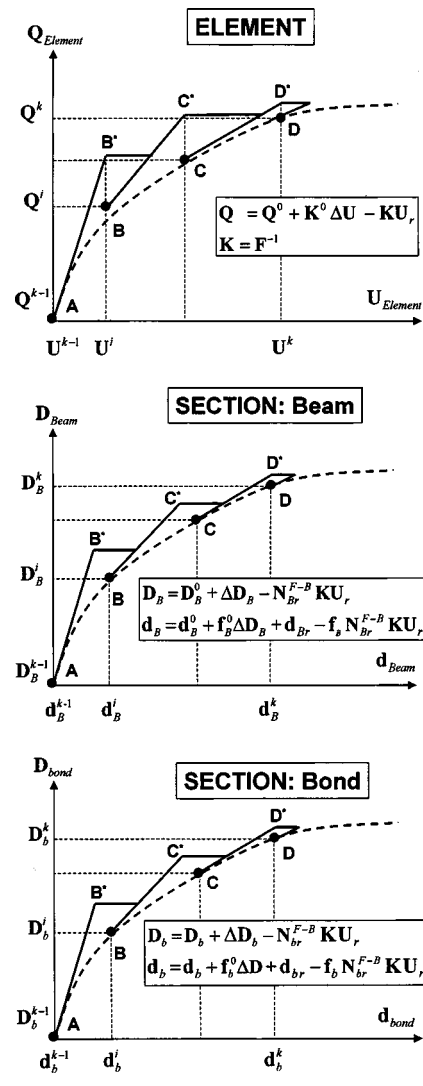


Fig. 3. Element state determination for force-based (hybrid) element

also shown in Fig. 4, which schematically represents the element, section, and bond state determinations.

In the first step, the element force increments $\Delta \mathbf{Q}_R$ are computed by linearizing the element force–deformation relation about the initial point (step a in Table 1, column 3). The current section forces \mathbf{D}_B are then computed via the force shape functions (step b). The section deformations \mathbf{d}_B are found by linearizing the force–deformation relation about the initial point 0, while the current bond deformations \mathbf{d}_b are computed from the current element nodal displacements \mathbf{U} through the displacement shape functions (step c). Based on the current section and bond deformations (\mathbf{d}_B and \mathbf{d}_b , respectively), the section state determinations are performed to compute the current section flexibility \mathbf{f}_B and the current bond stiffness \mathbf{k}_b , as well as the corresponding section \mathbf{D}_{Br} and bond \mathbf{D}_{br} resisting forces (step d). Next, the section residual deformations \mathbf{d}_{Br} are determined by transforming the section force unbalances ($\mathbf{D}_B - \mathbf{D}_{Br}$) through the section flexibility \mathbf{f}_B (step e).

Next, the beam contribution \mathbf{F}_B to the element flexibility is computed as the integral of the section flexibilities. The bond contribution \mathbf{K}_b to the element stiffness is computed as the integral of the bond stiffness along the element. The element stiffness \mathbf{K} is computed as the sum of the beam contribution (found by

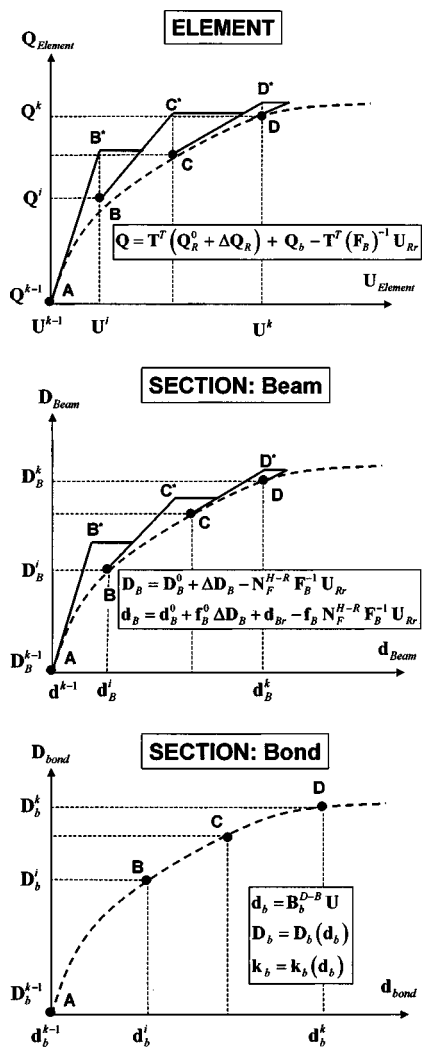


Fig. 4. Element state determination for Hellinger-Reissner mixed element

adding the rigid body modes to the inverse of F_B) and of K_b (step f). The nodal residual displacements U_{Rr} at the force degrees of freedom are computed based on the current section deformations d_B and element nodal displacements U (step g). The element forces Q are then updated (step h). As a result, the section forces D_B are updated using the force shape functions (step i). Finally, the section deformations d_B are updated to reflect the changes in the corresponding forces (step j).

Similarly to the force-based procedure, the element forces found with this procedure are not exact, but represent a first approximation. The “exact” forces are found when equilibrium at the nodal degrees of freedom is reached. At this point, the vector of residual deformations U_{Rr} approaches zero. If the hybrid procedure proposed by Spacone et al. (1996) is followed, the iterations continue by looping between steps d and j until U_{Rr} approaches zero. Only the beam section properties are updated during the iterations, while the bond deformations and forces do not change. Similarly to Fig. 3, points B^* , C^* , and D^* in Fig. 4 are the predictor points of the procedure, while points B , C , and D are the final, corrector points of the solution step.

In the proposed mixed state determination, equilibrium between the section forces and the nodal forces is satisfied pointwise through the beam force shape functions. Compatibility be-

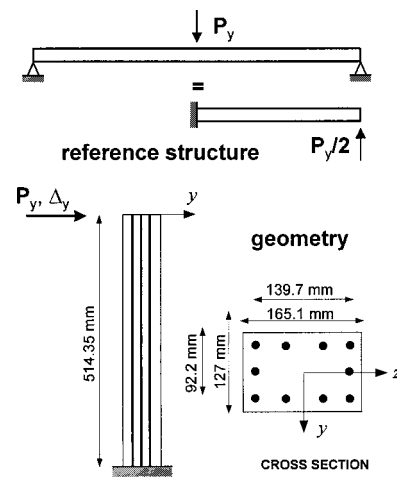


Fig. 5. Reinforced concrete reference structure

tween the section deformations and the nodal displacements is satisfied only in an integral sense. On the other hand, bond compatibility is satisfied pointwise, because the bond slips are computed through the displacement shape functions, while equilibrium between the bond forces and the nodal forces is only satisfied in an integral sense.

Numerical Validation

The performance of the three aforementioned RC frame elements with bond slip is investigated using the simply supported RC beam of Fig. 5. Because of symmetry, only half of the beam (the cantilever at the bottom of Fig. 5) is studied. The cantilever is a modified version of the specimen tested by Low and Moehle (1987) and used by Spacone and Limkatanyu (2000) to investigate the validity of the displacement-based element. The column cross section is divided into 20 layers. As shown in Fig. 5 the column cross section has ten No. 3 (bar diameter=9.5 mm) steel bars. Bond slip is allowed in all bars. The concrete base and the bars are assumed fixed at the column base, in order to simulate the zero axial displacement and zero rotation at midspan of the simply supported beam.

For the steel bars, $f_y = 447.5$ MPa and $E_s = 200,000$ MPa. For the concrete $f'_c = 36.5$ MPa for the unconfined concrete, and $f'_c = 42.1$ MPa for the confined core. The confined concrete compressive strength was found based on the work by Scott et al. (1982). The concrete tensile strength is neglected. Based on the set of formulas developed by Monti et al. (1994), the following characteristic values are used to describe the bond law. $u_b^1 = 0.254$ mm, $u_b^2 = 0.305$ mm, $u_b^3 = 1.27$ mm, $D_b^1 = 187.0$ kN/mm, and $D_b^3 = 62.4$ kN/mm. The notation of Fig. 2 in the companion paper (Limkatanyu and Spacone 2002) is used for the material parameters. The column is subjected to a monotonic lateral displacement inducing flexure about the weak axis y . Five Gauss-Lobatto integration points were used for the three elements.

Fig. 6 studies the number of elements needed to reach the converged solution for the three formulations by comparing the three load-displacement responses. The “exact” response is obtained with 32 displacement-based elements. The stiffness changes in the load-displacement responses are due to yielding of the reinforcing bars. Fig. 6(a) shows the response of the displacement-based element for an increasing number of elements

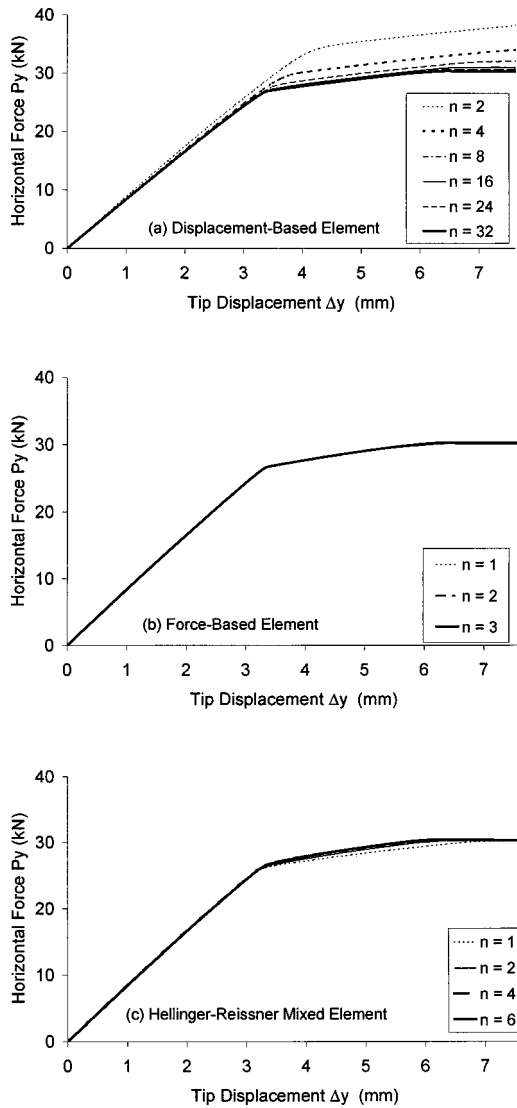


Fig. 6. Convergence study of three reinforced concrete elements

along the column. It is seen that for more than 16 elements the response does not change, indicating convergence of the solution. Fig. 6(b) shows that the force-based element is much more accurate, and only one element is necessary to reach convergence. Similarly, Fig. 6(c) shows that the Hellinger–Reissner mixed element is also quite accurate, as evidenced by the increase in precision after yielding of the first bar for two, four, and six elements.

It is noteworthy to point out that for the displacement-based element an increase in the number of elements results in a more flexible response (convergence from above), while for the Hellinger–Reissner mixed element, in which the axial and flexural behaviors derive from the force shape functions, an increase in the number of elements leads to stiffer responses (convergence from below). The force-based element also converges from below, but the figure scale hides this phenomenon. Convergence from below in the Hellinger–Reissner mixed element and its high precision, closer to that of the force-based element, show how the force-shape functions \mathbf{N}_F^{H-R} play a role that is more important than that of the displacement shape functions \mathbf{N}_u^{H-R} in determining the element accuracy. Based on the results of Fig. 6, the computational times central processing unit (CPU) time on a P700 per-

Table 2. Central Processing Unit Time (on P700 PC) and Number of Elements Needed for Convergence for Beam of Fig. 5

Number of elements	Displacement-based		Force-based		Hellinger–Reissner	
	CPU Time (s)	Error (%)	CPU Time (s)	Error (%)	CPU Time (s)	Error (%)
1	0.95	(49.80)	1.85	(0.22)	1.07	(1.50)
2	1.70	(16.50)	converged		2.20	(0.62)
4	2.77	(6.65)	converged			
8	5.46	(2.81)	converged			
16	10.68	(1.08)	converged			
17	11.71	(0.98)	converged			

sonal computer and errors of the three aforementioned RC frame elements with different numbers of elements are summarized in Table 2. The errors were measured by the following expression:

$$E = \frac{\sum_{k=1}^{N_{\text{step}}} \left| \frac{P_{y_k} - P_{y_k}^{\text{exact}}}{P_{y_k}^{\text{exact}}} \right|}{N_{\text{step}}} \times 100 \quad (1)$$

where E = the percentage error, N_{step} = the number of applied displacement steps used in the analysis (this number is the same for all analyses of Fig. 6), P_{y_k} = the horizontal forces at step k , and $P_{y_k}^{\text{exact}}$ = the “exact” forces at the same step. The results of Table 2 confirm the better accuracy of the force-based and Hellinger–Reissner mixed elements with respect to the computational cost of the analyses. The CPU time of a single force-based element is basically twice that of a single displacement-based element, while the CPU time of the mixed element is comparable to that of the displacement-based element. A further study compares the CPU time necessary to reach convergence. Convergence is defined when the above-defined error E is smaller than 1%. The use of force-based elements leads to the lowest CPU time (because only one element is needed), while the displacement-based elements lead to the slowest solution (because 17 elements are needed to reach convergence). Two mixed elements are needed to reach convergence, with a convergence time slightly higher than that of the force-based element.

The curvature and moment distributions at the integration points along the column corresponding to a tip displacement $\Delta_y = 7.62$ mm are shown in Figs. 7(a and b), respectively. The responses of two force-based elements and two H–R mixed elements are compared. The response with 32 displacement-based elements is used as reference solution. Two elements are sufficient to obtain a good representation of the response with both force-based and H–R mixed elements. Fig. 7(a) shows the curvature distribution, which is truncated at 0.003 mm/mm because the large curvature jump at the column base does not allow us to show the details of the element characteristics.

For the displacement-based element, Figs. 7(a and b) show discontinuities in the curvature and moment distributions between adjacent elements, because in this formulation there is neither compatibility nor equilibrium between two end sections in two adjacent elements. Similar discontinuities are observed in the curvature and force distributions obtained with two H–R mixed elements, because the nodal force degrees of freedom are condensed out, as outlined in the companion paper (part I). The jump in the

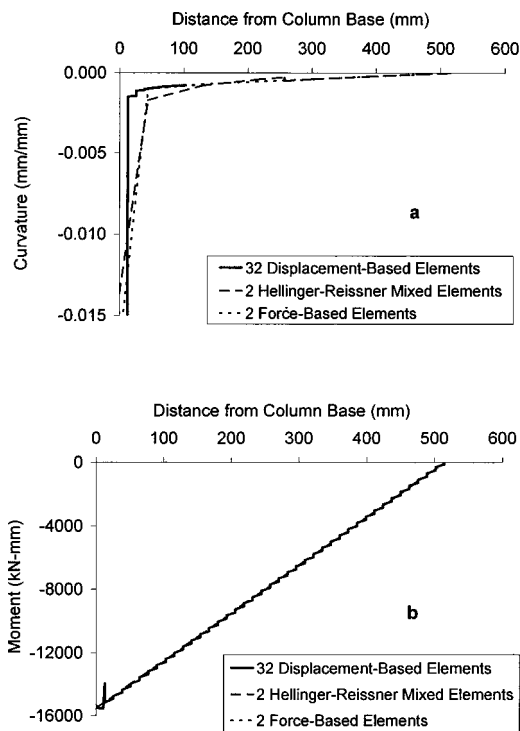


Fig. 7. Curvature and moment distributions at integration points for tip displacement $\Delta_y = 7.62$ mm

moment distribution for two H–R mixed elements is quite small in Fig. 7(b) and is not clearly visible. Higher order force shape functions would lead to larger moment discontinuities between adjacent mixed elements (Ayoub and Filippou 2000). On the other hand, the curvature and moment distributions obtained with two force-based elements are continuous. This derives from the fact that since the nodal forces are in equilibrium, and because the internal force distributions are in equilibrium with the nodal forces through the force shape functions, the internal force distributions are continuous. Because the section deformations in the force-based element are obtained from the section forces through the section constitutive law, the section deformations (curvature in this case) are also continuous.

It is noteworthy to emphasize that the moment variation along the cantilever column subjected only to a tip lateral load is linear. However, the moment distribution with 32 displacement-based elements of Fig. 7(b) shows a zigzagged shape, because equilibrium is only imposed in an integral sense inside the displacement-based element. Furthermore, a jump in the moment is observed near the column base, due to numerical instabilities already observed in previous studies on displacement-based elements for steel–concrete composite beams with deformable shear studs (Ayoub and Filippou 2000). On the other hand, the moment distributions produced by both the force-based elements and the H–R mixed elements are linear. Similar conclusions to those drawn from Fig. 7 on the curvature and moment distributions along the cantilever apply to the axial strain and axial force distributions.

Fig. 8 shows the bond force distributions in the top steel bars corresponding to tip displacements Δ_y of 2.54, 3.81, and 7.62 mm. The 2.54, 3.81, and 7.62 mm tip displacements correspond to three different states of stress in the steel bars at the column base. When $\Delta_y = 2.54$ mm, all steel bars are still in the linear elastic range. When $\Delta_y = 3.81$ mm, the top steel bars have

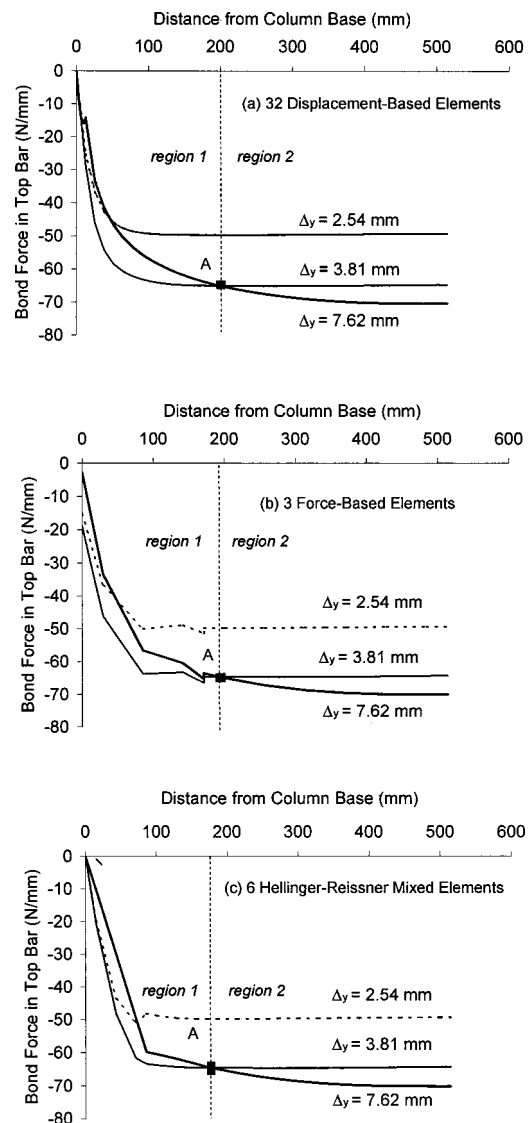


Fig. 8. Bond force distributions in top steel bars at different tip displacement Δ_y

yielded, and when $\Delta_y = 7.62$ mm both the top and middle steel bars have yielded. In order to obtain a sufficiently accurate representation of the bond force distributions in the steel bars, the number of elements is increased from two to six for the H–R mixed element and from one to three for the force-based element. Using displacement-based and H–R mixed elements, satisfaction of the bond compatibility in a pointwise, strong sense leads to continuous bond-slip and bond force distributions between adjacent elements, while the results obtained using force-based elements show discontinuous bond force and bond-slip distributions between adjacent elements, because the reference bond forces are condensed out. Clearly, only three force-based elements and six H–R mixed elements adequately represent the bond force distributions obtained with 32 displacement-based elements. For the displacement-based and H–R mixed elements, the bond forces at the column base are equal to zero because bond compatibility is imposed pointwise. On the other hand, bond compatibility is only imposed in an integral sense in the force-based formulation. This leads to nonzero bond forces at the column base, even though there is no nodal slip. It is interesting to observe that for $\Delta_y = 3.81$ and 7.62 mm, the bond stresses decrease before point A

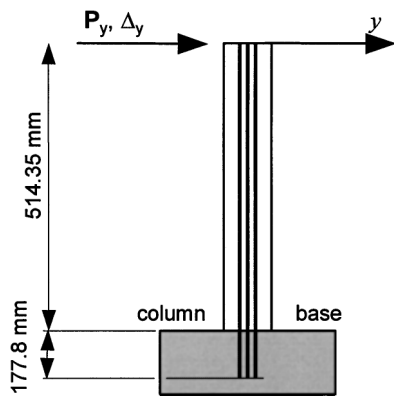


Fig. 9. Reinforced concrete column with anchorage zone

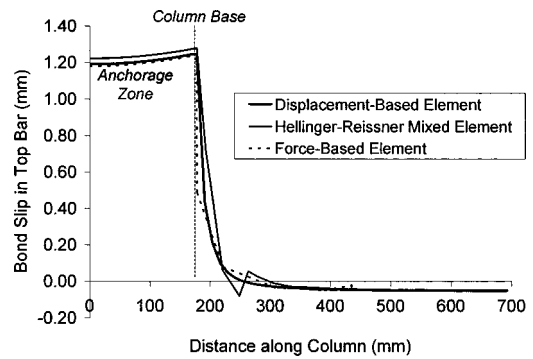


Fig. 11. Bond-slip distribution in top bar of reinforced concrete column of Fig. 9 ($\Delta_y = 7.62$ mm)

(region 1) and increase after point A (region 2). This happens because in region 1 the steel stresses in the top bars are in the transient part between the elastic and the perfectly plastic branches, while in region 2 the steel stresses in the top bars are still in the linear elastic region. The steel modulus in the transient part drastically decreases from the elastic value to zero, hence leading to a decrease in the bond forces in region 1.

In order to investigate the capability of the proposed RC frame elements to detect the bar pullout and the resulting load-displacement softening response, the anchorage zone was introduced below the column base to reflect the geometric dimensions of the specimen tested by Low and Moehle (1987). All the steel bars were extended 177.8 mm into the anchorage block. The bar ends are free to slip in order to represent the pullout failure. In the current study, all the bars have an identical diameter, while three different bar sizes were used in the original specimen by Low and Moehle (1987). The specimen geometry is shown in Fig. 9. The concrete is assumed rigid in the anchorage block.

The load-displacement diagram obtained with the three elements is shown in Fig. 10. For the displacement-based mesh, there are 32 elements in the column and seven elements in the anchorage zone. For the force-based element mesh, two elements are used in the column and two elements in the anchorage zone. Finally, six elements in the column and seven elements in the anchorage zone are used in the H-R element mesh. Similarly to the procedure of Fig. 6, the above meshes were obtained by refining the mesh for each element type, until convergence was reached in the response. The bond-slip distributions in the top bars corresponding to a tip displacement $\Delta_y = 8.9$ mm are shown in Fig. 11. As expected, the maximum slip occurs at the column

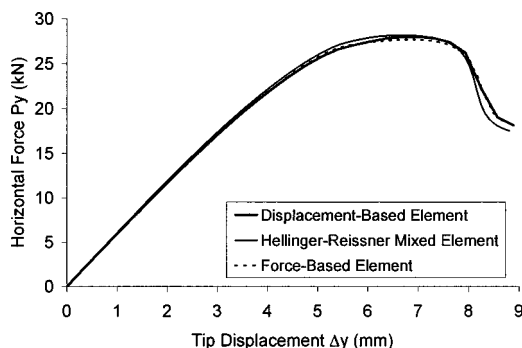


Fig. 10. Load-displacement response of reinforced concrete column of Fig. 9

base. It is also evident that the entire bar anchorage length has pulled out from the foundations. Consequently, the pullout failure in the top bars along the anchorage results in a reduction of the load-carrying capacity of the column. The three proposed elements succeeded in detecting the pullout failure. The force-based element shows an advantage in terms of overall computational cost. However, it is important to point out that the force-based element mesh showed some numerical instabilities during the studies that led to a lack of structural convergence in some cases. This is due to the fact that the bond stiffness matrix needs to be inverted during the element state determination. When the bars pull out, the bond constitutive law reaches a plateau of zero stiffness, thus leading to a singular stiffness matrix that cannot be inverted. Once the slips pass the peak and start softening, the bond tangent stiffness matrix becomes negative definite and is inverted without problems. On the other hand, both the displacement-based and the H-R element meshes did not show such problems, because the bond behavior is derived from the displacement shape functions, and thus the bond-slip stiffness does not need to be inverted.

Summary and Conclusions

The state determination of the proposed displacement-based RC element is a lot simpler than those of the force-based and the mixed formulations. However, this paper shows the far superior precision of the force-based and of the Hellinger-Reissner mixed elements. Even though a single displacement-based element is much faster than the other two elements, a mesh of several displacement-based elements (which requires high computational times) is needed to reach an accurate result. On the other hand, force-based and mixed elements are computationally more demanding, but their accuracy leads to the use of far fewer elements per structural member to reach a converged solution, thus yielding a noticeable computational saving when compared with meshes of displacement-based elements. The numerical tests performed in this paper show that the force-based element is slightly more accurate than the mixed element.

In the displacement-based element, the bond force and the slip distributions are continuous over adjacent elements due to the

strong satisfaction of the bond compatibility, while the internal force and deformation distributions are discontinuous between adjacent elements due to the weak satisfaction of the equilibrium conditions. In the force-based element, the bond force and the bond-slip distributions over adjacent elements are discontinuous due to the condensation of the element bond forces, while the internal force and deformation distributions are continuous over adjacent elements due to the enforcement of equilibrated force shape functions. In the Hellinger–Reissner mixed element, the bond force and the bond-slip distributions over adjacent elements are continuous due to the strong satisfaction of the bond compatibility, while the internal force and deformation distributions are discontinuous over adjacent elements due to the condensation of the element force degrees of freedoms.

The example of a RC cantilever column with insufficient anchorage length in the rebars is used to test the elements' capability of representing the softening response of a RC member with bar pullout. While all three elements can trace the softening response of the column, the force-based and mixed elements are far more precise. During the analyses it was observed that the force-based element has some numerical problems when the bars start pulling out. This is due to the fact that the force-based state determination requires inversion of the bond stiffness matrix. This matrix becomes singular when the bars start pulling out. On the other hand, both the displacement-based and the Hellinger–Reissner mixed elements easily pass this point, because their state determinations do not require inversion of the bond stiffness matrix.

The development of the proposed RC elements with bond slip is a step forward in establishing a computational framework that permits the nonlinear static and dynamic analysis of RC frames, including the effects of bond slip. The next step in this direction is to develop node elements that allow the connection between different frame elements, in particular beam-to-column elements.

Acknowledgments

This study was supported by the Royal Thai Fellowship and by Grant No. CMS-9804613 from the National Science Foundation. This support is gratefully acknowledged. Any opinions expressed in this paper are those of the writers and do not reflect the views of the sponsoring agencies.

References

- Ayoub, A., and Filippou, F. C. (2000). "Mixed formulation of nonlinear steel-concrete composite beam element." *J. Struct. Eng.*, 126(3), 371–381.
- Ciampi, V., and Carlesimo, L. (1986). "A nonlinear beam element for seismic analysis of structures." *Proc., 8th European Conf. on Earthquake Engineering*, Lisbon, Portugal, 73–80.
- Kaba, S., and Mahin, S. A. (1984). "Refined modeling of reinforced concrete columns for seismic analysis." *Rep. EERC 84-03*, Earthquake Engineering Research Center, Univ. of California, Berkeley, Calif.
- Limkatanyu, S., and Spacone, E. (2002). "R/C frame element with bond interfaces. Part I: displacement-based, force-based and mixed formulations." *J. Struct. Eng.*, 128(3), 346.
- Low, S. S., and Moehle, J. P. (1987). "Experimental study of reinforced concrete columns subjected to multi-axial cyclic loading." *Rep. EERC 87/14*, Earthquake Engineering Research Center, Univ. of California, Berkeley, Calif.
- Mahasuverachai, M., and Powell, G. H. (1982). "Inelastic analysis of piping and tubular structures." *Rep. EERC 82/27*, Earthquake Engineering Research Center, Univ. of California, Berkeley, Calif.
- Monti, G., De Sortis, A., and Nuti, C. (1994). "Problemi di scala nella sperimentazione pseudodinamica di pile da ponte in C.A." *Proc., Workshop Danneggiamento, Prove Cicliche e Pseudodinamica, (Damage, Cyclic Tests and Pseudo-dynamic Testing)*, Napoli, Italy (in Italian).
- Neuenhofer, A., and Filippou, F. C. (1997). "Evaluation of nonlinear frame finite-element models." *J. Struct. Eng.*, 123(7), 958–966.
- Salari, M. R., Spacone, E., Shing, P. B., and Frangopol, D. M. (1998). "Nonlinear analysis of composite beams with deformable shear connectors." *J. Struct. Eng.*, 124(10), 1148–1158.
- Scott, B. D., Park, R., and Priestley, M. J. N. (1982). "Stress–strain behavior of concrete confined by overlapping hoops at low and high strain rates." *ACI Struct. J.*, 79(1), 13–27.
- Spacone, E., Filippou, F. C., and Taucer, F. F. (1996). "Fibre beam-column model for nonlinear analysis of RC frames. Part I: formulation." *Earthquake Eng. Struct. Dyn.*, 25, 711–725.
- Spacone, E., and Limkatanyu, S. (2000). "Response of reinforced concrete members including bond-slip effects." *ACI Struct. J.*, 97(6), 831–839.
- Taylor, R. L. (2000). *FEAP: A finite element analysis program, user manual: version 7.3*, Dept. of Civil and Environmental Engineering, Univ. of California, Berkeley, Calif. (<http://www.ce.berkeley.edu/~rlt/feap/>)
- Zeris, C. A., and Mahin, S. A. (1988). "Analysis of reinforced concrete beam-columns under uniaxial excitation." *J. Struct. Eng.*, 114(ST4), 804–820.
- Zeris, C. A., and Mahin, S. A. (1991). "Behavior of reinforced concrete structures subjected to biaxial excitation." *J. Struct. Eng.*, 117(ST9), 2657–2673.